MUSCULOSKELETAL

Whole-tumor histogram analysis of diffusion-weighted imaging and dynamic contrast-enhanced MRI for soft tissue sarcoma: correlation with HIF-1alpha expression

Xiangwen Li[1] · Yiwen Hu[1] · Yuxue Xie[1] · Rong Lu[1] · Qing Li[2] · Hongyue Tao[1] · Shuang Chen[1,3]

Abstract

Objective To investigate the correlation of histogram metrics from diffusion-weighted imaging (DWI) and dynamic contrast-enhanced magnetic resonance imaging (DCE-MRI) parameters with HIF-1alpha expression in soft tissue sarcoma (STS).

Methods We enrolled 71 patients with STS who underwent 3.0-T MRI, including conventional MRI, DWI, and DCE-MRI sequences. Location, maximum tumor diameter, envelope, T2-weighted tumor heterogeneity, peritumoral edema, peritumoral enhancement, necrosis, tail-like pattern, bone invasion, and vessel/nerve invasion and/or encasement were determined using conventional MRI images. The whole-tumor histogram metrics were calculated on the apparent diffusion coefficient (ADC), K^{trans}, K_{ep}, and V_e maps. Independent-samples t test and one-way ANOVA were used for testing the differences between normally distributed categorical data with HIF-1alpha expression. Pearson and Spearman correlations and multiple linear regression analyses were performed to determine the correlations between histogram metrics and HIF-1alpha expression. Survival curves were plotted using the Kaplan-Meier method.

Results Regarding conventional MRI features, only highly heterogeneous on T2-weighted images (55.6 ± 19.9% vs. 45.4 ± 20.5%, $p = 0.041$) and more than 50% necrotic area (57.3 ± 20.4% vs. 43.9 ± 19.7%, $p = 0.002$) were prone to indicate STS with higher HIF-1alpha expression. Histogram metrics obtained from ADC (mean, median, 10th, and 25th percentile values), K^{trans} (mean, median, 75th, and 90th percentile values), and K_{ep} (90th percentile values) were significantly correlated with HIF-1alpha expression. Multiple linear regression analysis demonstrated that more than 50% necrosis, $ADC_{skewness}$, K^{trans}_{90th}, and grade III were independently associated with HIF-1alpha expression.

Conclusion DWI and DCE-MRI histogram parameters were significantly correlated with HIF-1alpha expression in STS.

Key points
• *DWI and DCE-MRI histogram parameters are correlated with HIF-1alpha expression in STS.*
• *More than 50% necrosis, $ADC_{skewness}$, K^{trans}_{90th}, and grade III were independently associated with HIF-1alpha expression in STS.*

Keywords Diffusion magnetic resonance imaging · Magnetic resonance imaging · Sarcoma · Hypoxia-inducible factor 1

Abbreviations

DCE	Dynamic contrast-enhanced
DWI	Diffusion-weighted imaging
HIF	Hypoxia-inducible factor
ICC	Intraclass correlation coefficient
MRI	Magnetic resonance imaging
ROC	Receiver operating characteristic
STS	Soft tissue sarcoma

Xiangwen Li, Yiwen Hu, Yuxue Xie and Rong Lu contributed equally to this work.

✉ Hongyue Tao
taohongyue@126.com

✉ Shuang Chen
chenshuang6898@126.com

[1] Department of Radiology and Institute of Medical Functional and Molecular Imaging, Huashan Hospital, Fudan University, 12 Wulumuqizhong Road, Shanghai, China

[2] MR Collaborations, Siemens Healthineers Ltd., Shanghai, China

[3] National Clinical Research Center for Aging and Medicine, Huashan Hospital, Fudan University, 2 middle Wulumuqizhong Road, Shanghai, China

TE   Echo time
TR   Repetition time
TIC   Time-signal intensity curve

Introduction

Soft tissue sarcomas (STS) are highly heterogeneous malignant tumors originating from mesenchymal components [1]. Due to the high mortality and recurrence rates, scholars have preferred evaluating the relationship between the internal microenvironmental state and patient clinical outcomes [2–4]. Tumor angiogenesis is an essential biological behavior of soft tissue sarcoma, which provides oxygen and nutrients to tumor cells and plays a vital role in tumor proliferation, metastasis, and prognosis [5, 6]. The hypoxic state is the switch for angiogenesis. Among all molecules that sense hypoxia and respond to it, hypoxia-inducible factor-1alpha (HIF-1alpha) is the most critical factor regulating oxygen homeostasis [7].

Under hypoxic conditions, HIF-1alpha degradation is inhibited; subsequently, HIF-1alpha binds to hypoxia-responsive elements in the promoter regions of target genes such as erythropoietin and vascular endothelial growth factor to promote tumor angiogenesis and induce tumor progression [8–10]. Although HIF-1alpha has not been incorporated into the treatment strategy for STS, several studies have reported the potential of HIF-1alpha as a possible prognostic marker for STS [11–13]. In addition, it has been suggested that high HIF-1alpha status may lead to a higher level of drug resistance in STS [14, 15].

Currently, we usually use puncture biopsies to obtain histopathological information about the tumor preoperatively; however, due to the highly heterogeneous nature of sarcoma composition, puncture biopsy may underestimate the proper level of histological expression within the tissue due to sampling error. Magnetic resonance imaging (MRI) has been widely used for imaging-pathology control studies of malignant tumors due to its high soft tissue resolution and multi-sequence imaging. Several quantitative functional MRI methods have been used to assess tumor oxygenation status, such as blood oxygenation level–dependent–based functional MRI (BOLD-fMRI), diffusion-weighted imaging (DWI), and dynamic contrast-enhanced MRI (DCE-MRI) methods [16–18]. BOLD-fMRI can be used to assess tumor oxygenation levels. However, the need for oxygen breathing during BOLD-fMRI image acquisition is cumbersome and unsuitable for routine clinical application [19]. DWI can indirectly reflect the oxygenation status of tumors by the level of cellularity in the hypoxic state, and its derived parameter apparent diffusion coefficient (ADC) value is significantly correlated with HIF-1alpha [20]. Furthermore, several researchers have demonstrated that quantitative parameters generated by

pharmacokinetic modeling with DCE-MRI may predict HIF-1alpha expression through the level of tumor blood supply [21, 22]. However, the reflection of quantitative parameters on HIF-1alpha expression levels seems controversial among different histological types of tumors. In cervical and ovarian cancer, there appear to be positive correlations between HIF-1alpha and DCE-MRI perfusion parameters, while other studies reported reverse conclusions [23–26]. There is also disagreement about the ability of ADC values to predict HIF-1alpha expression [27–29]. Thus, any single imaging method is not sensitive enough to reflect the tumor oxygenation status. In contrast, the combined application of multiparametric imaging is expected to play a more critical role in assessing tumor hypoxia. Besides, most previous studies reflected the tissue microstructure of STS by measuring the region of interest (ROI) [30, 31]. However, the tissue components within the STS are highly heterogeneous, and small ROI measurements of tumors do not fully reflect the heterogeneity of cancer. Conversely, whole-tumor histogram analysis is a method that provides more objective and accurate quantitative information about tissue characteristics and heterogeneity, with minimal inter-reader variability [32, 33].

Therefore, the purpose of this study was to correlate quantitative parameters from DWI and DCE-MRI with HIF-1alpha in STS using whole-tumor histogram analysis and to identify independent factors that could be used to predict HIF-1alpha expression.

Materials and methods

This prospective study was approved by the Health Sciences Institutional Review Board (HIRB, 2019 M-010) of Huashan Hospital Fudan University. Informed consent was obtained from all patients.

Study population

From January 2019 to January 2021, 150 patients with suspected soft tissue tumors were recruited into our institution for treatment. All patients underwent a 3.0-T MRI scanning protocol preoperatively and underwent radical resection to obtain tumor specimens for histopathological analysis. The following exclusion criteria were used in this study: (1) benign or intermediate soft tissue tumors; (2) MRI images with severe motion artifacts; (3) patients who underwent only puncture biopsy; and (4) interval between MRI examination and surgery of more than 2 weeks.

The following covariates were reported: age, sex, presence of local pain, histological type confirmed by surgery, FNCLCC grading, postoperative adjuvant radiotherapy, postoperative adjuvant chemotherapy, and occurrence of recurrence (local and metastatic) or death. Routine follow-up

included clinical physical examination, chest CT thin-section (1 mm) examination, and MRI examination of the operative area. This was done every 3 months for 3 years. All abnormal findings required histopathological confirmation. The overall survival (OS) was defined as the time from the initial pathological diagnosis to death. Disease-free survival (DFS) was defined as the time between the start of randomization and disease recurrence or death from any cause.

MRI examination protocol

All MRI examinations were performed using a 3.0-T (Verio; Siemens) MRI scanner. Conventional MRI protocols included axial and coronal fast spin-echo T1-weighted (repetition time (TR)/echo time (TE) = 445–883/13–19 ms; slice thickness = 3–7 mm) image and fat suppression T2-weighted (T2WI) (TR/TE = 3002–5428/70–82 ms, slice thickness = 3–7 mm) image in the axial and sagittal plane.

Axial-plane DWI images were acquired using a single spin-echo echo-planar imaging sequence with two b values (0, 800 s/mm^2). The parameters were TR = 5000 ms; TE = 61–70 ms; layer thickness = 3–7 mm; and number of excitations, 2. The total acquisition time was 188 s.

DCE-MRI was performed using an acquisition with a volumetric interpolated breath-hold examination sequence based on a three-dimension T1-weighted fast-spoiled gradient echo technique. The parameters were as follows: flip angle = 3°, 6°, 9°, and 12°; layer thickness = 3–7 mm; layer spacing = 0 mm; TR = 5.0 ms; and TE = 1.7 ms. Before the injection of contrast material, three cycles were pre-scanned to calculate baseline T1 maps. From the fourth cycle, dynamic enhancement scans were performed using a high-pressure syringe injection of gadoterate meglumine (Dotarem®; Guerbet) at a rate of 2.5 mL/s and a dose of 0.1 mmol/kg, followed by a 20-mL physiological saline flush tube with a flow rate of 2 mL/s. A total of 40 cycles were scanned for 8 s each. The total acquisition time was 320 s.

MR image analysis

Consensual review of all conventional MRI, DWI, and DCE-MRI images was performed by two musculoskeletal radiologists with 10 and 20 years of experience who were blinded to the clinical and pathological information.

The following qualitative tumor signs were recorded: (*a*) location; (*b*) maximum tumor diameter; (*c*) envelope; (*d*) T2WI tumor heterogeneity; (*e*) peritumoral edema; (*f*) peritumoral enhancement; (*g*) necrosis; (*h*) tail-like pattern; (*i*) bone invasion; (*j*) vessel invasion and/or encasement; and (*k*) nerve invasion and/or encasement. The exact definition of qualitative signs of the tumor is mentioned in Supplementary material S1.

DWI images were analyzed using Advantage Workstation 4.7 (GE Healthcare). MADC software was used for fitting to generate ADC maps. After adjusting the threshold and removing background noise, a single exponential model was selected to generate ADC maps.

For data extraction, DCE-MRI images were transferred to a Siemens imaging workstation (Syngo; B17). Tissue 4D software was used for data post-processing. Based on the extended Tofts hemodynamic model, the personalized arterial input function (AIF) and population-averaged AIF method were chosen to estimate quantitative parameters separately. Time-signal intensity curve (TIC) types (four types [34]), K^{trans}, K_{ep}, and V_e maps were obtained for each lesion by two readers. The following permeability model was performed: $K_{ep} = K^{trans}/V_e$ [35]. The exact definition of DCE-MRI features was demonstrated in Supplementary material S2.

The 3D Slicer (v. 5.0.2; http://www.slicer.org) software was used to perform histogram analysis. For each lesion, two radiologists drew irregular volume of interest (VOI) layer by layer along the outer edge of the tumor on each ADC map to cover the whole tumor concerning the T2-weighted and contrast-enhanced T1-weighted images. Subsequently, the entire tumor VOI was copied and pasted onto the K^{trans}, K_{ep}, and V_e maps. Eight histogram metrics were obtained from each parametric map, including mean, median, 10th, 25th, 75th, and 90th percentile values, skewness, and kurtosis.

Pathological and immunohistochemical evaluation

Histopathological diagnosis (histological types and FNCLCC grading) and immunohistochemical staining analysis of each lesion were reviewed by pathologists with more than 10 years of experience in sarcoma diagnosis. The histopathological diagnosis based on the examination of resected surgical specimens was by the WHO Soft Tissue Tumor Classification (2020 version). Detailed methods for assessing HIF-1alpha expression are illustrated in Supplementary material S3.

Statistical analysis

Detailed statistical methods are presented in Supplementary material S4.

Results

Seventy-one patients were included in the final analysis, including 40 males (mean age, 58 years) and 31 females (mean age, 61 years). Twenty-one lesions were located in the thigh, 11 in the calf, 8 in the knee, 9 in the shoulder, 12 in the forearm, 6 in the upper arm, and four in the back. The most common histological types were undifferentiated pleomorphic sarcoma (17/71, 23.9%), pleomorphic liposarcoma (12/71,

Fig. 1 Distribution of HIF-1alpha expression of the patients
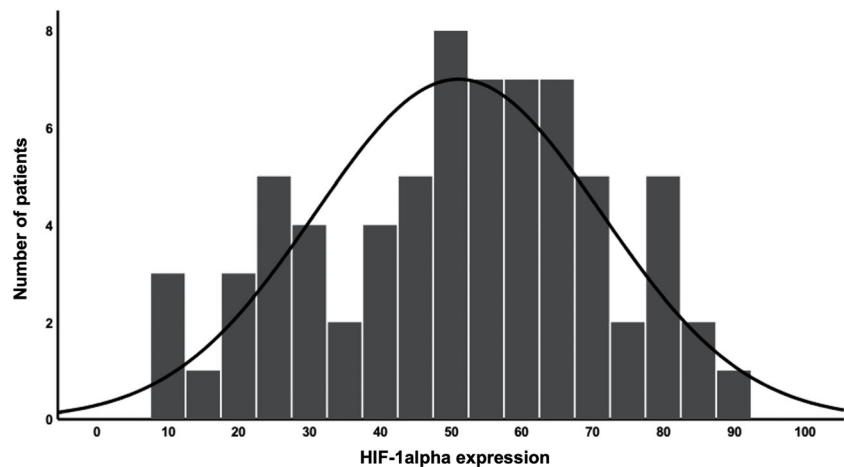
16.9%), and fibrosarcoma (12/71, 16.9%). The expression of HIF-1alpha-positive cells ranged from 10 to 90%, with median and quartiles of 35%, 55%, and 65%, respectively (Fig. 1). In this study, 15 (21.1%) had grade I STS, 29 (40.8%) had grade II STS, and 27 (38.0%) had grade III STS.

On comparing clinical features, no significant differences in HIF-1alpha expression were observed between different groups regarding sex, age, location, and tumor size. No significant differences in HIF-1alpha expression were observed between different histological types. However, there were significant differences in HIF-1alpha expression between histological grades, with HIF-1alpha expression increasing with higher histological grades.

For MRI qualitative variables, the interobserver agreement showed moderate to almost perfect agreement ($\kappa = 0.54$–0.84) (Supplementary material Table 1). Among all MRI qualitative features, only highly heterogeneous on T2WI images (55.6 ± 19.9% vs. 45.4 ± 20.5%, $p = 0.041$) and more than 50% necrotic area (57.3 ± 20.4% vs. 43.9 ± 19.7%, $p = 0.002$) were prone to indicate STS with higher HIF-1alpha expression. Still, envelope, peritumoral edema, peritumoral enhancement, tail-like pattern, bone invasion, and vessel/nerve invasion and/ or encasement were not (Table 1).

Figure 2 shows the scatterplots and Bland-Altman plots of the personalized AIF method versus the population-averaged AIF method calculated for the DCE-MRI parameters. Finally, the personalized AIF method was chosen. Interobserver agreements for histogram metrics of DWI and DCE-MRI parameters were moderate to good agreement. The ICC values ranged from 0.826 to 0.966 (Table 2). The measurements of histogram metrics derived from DWI and DCE-MRI parameters are shown in Table 3. The correlations of histogram metrics derived from DWI and DCE-MRI parameters with HIF-1alpha expression of STS are summarized in Table 4. ADC's mean, median, 10th, and 25th percentile values were

negatively correlated with HIF-1alpha expression, while ADC$_{skewness}$ was most significantly positively correlated with HIF-1alpha expression ($r = 0.526$, $p < 0.001$). Histogram metrics obtained from K^{trans} (mean, median, 75th, and 90th percentile values) were significantly positively correlated with HIF-1alpha expression. $K^{trans}_{skewness}$ was moderate negatively correlated with HIF-1alpha expression ($r = -0.352$, $p < 0.001$). For K_{ep}, only the 90th percentile value was observed to present a moderate positive correlation with HIF-1alpha expression ($r = 0.331$, $p = 0.026$). Furthermore, V_e-derived histogram metrics were not associated with HIF-1alpha expression. Figures 3 and 4 show typical histogram distributions of DWI and DCE-MRI maps in the presence of lower- and higher-HIF-1alpha expression cases (Fig. 4).

T2WI tumor heterogeneity, necrotic area, significant DWI and DCE-MRI histogram metrics, and clinical and pathological features (histological type and FNCLCC grade) were included in the multiple linear regression analysis to determine the independent parameters for the characterization of HIF-1alpha expression in STS. More than 50% necrosis, ADC$_{skewness}$, K^{trans}_{90th}, and grade III were independently associated with HIF-1alpha expression (standardized β coefficient for more than 50% necrosis = 0.074, $p = 0.011$; for ADC$_{skewness}$ = -0.332, $p = 0.003$; for K^{trans}_{90th} = 0.203, $p = 0.027$; for grade III = 0.314, $p = 0.004$) (Table 5).

KM survival analysis is demonstrated in Fig. 5 and Supplementary material S5, Supplementary material Table 2, and Supplementary material Table 3.

Discussion

This study used whole-tumor histogram analysis to reveal that DWI and DCE-MRI parameters correlated with HIF-1alpha

Table 1 Descriptive statistics and distribution of clinical and MRI features according to tumor HIF-1alpha expression level

Characteristics	Distribution frequency	Mean HIF-1alpha expression (%)	*p* value
Gender			0.658
Male	43.7 (31/71)	49.8 ± 22.5	
Female	56.3 (40/71)	52.0 ± 18.5	
Age			0.652
< 50 years old	39.4 (28/71)	52.1 ± 21.6	
≥ 50 years old	60.6 (43/71)	50.1 ± 19.3	
Location			0.848
Deep	45.1 (32/71)	49.5 ± 20.2	
Superficial	36.6 (26/71)	52.1 ± 19.5	
Deep and superficial	18.3 (13/71)	52.7 ± 23.0	
Maximum tumor diameter			0.784
< 5 cm	29.6 (21/71)	40.2 ± 16.8	
5–10 cm	40.8 (29/71)	54.3 ± 19.9	
> 10 cm	29.6 (21/71)	57.4 ± 20.3	
Envelope			0.387
Absent	74.6 (53/71)	49.3 ± 19.7	
Present	25.4 (18/71)	53.5 ± 21.1	
T2WI tumor heterogeneity			0.041*
Slightly heterogeneous	49.3 (35/71)	45.4 ± 20.5	
Highly heterogeneous	50.7 (36/71)	55.6 ± 19.9	
Peritumoral edema			0.568
Absent	47.9 (34/71)	49.5 ± 18.1	
Present	52.1 (37/71)	52.3 ± 22.0	
Peritumoral enhancement			0.150
Absent	50.7 (36/71)	47.6 ± 19.6	
Present	49.3 (35/71)	54.6 ± 20.5	
Necrosis			0.002*
< 50% necrosis	62.0 (44/71)	43.9 ± 19.7	
≥ 50% necrosis	38.0 (27/71)	57.3 ± 20.4	
Tail-like pattern			0.461
Absent	62.0 (44/71)	49.7 ± 21.2	
Present	38.0 (27/71)	53.3 ± 18.7	
Bone invasion			0.718
Absent	73.2 (52/71)	47.8 ± 19.5	
Present	26.8 (19/71)	52.6 ± 22.1	
Vessel invasion and/or encasement			0.799
Absent	57.7 (41/71)	51.6 ± 20.6	
Present	42.3 (30/71)	50.3 ± 20.0	
Nerve invasion and/or encasement			0.577
Absent	66.2 (47/71)	52.0 ± 20.6	
Present	33.8 (24/71)	49.2 ± 19.7	
TIC curve types			0.518
I	11.3 (8/71)	38.8 ± 13.6	
II	31.0 (22/71)	43.0 ± 20.3	
III	36.6 (26/71)	55.6 ± 20.1	
IV	21.1 (15/71)	61.7 ± 16.1	

T2WI T2-weighted, *TIC* time-signal intensity curve

*The result is statistically significant

Table 2 Inter-reader reproducibility for ADC, K^{trans}, K_{ep}, and V_e measurements

	DWI	DCE-MRI		
	ADC	K^{trans}	K_{ep}	V_e
10th	0.845 (0.721–0.897)	0.855 (0.773–0.902)	0.881 (0.812–0.923)	0.861 (0.781–0.912)
25th	0.921 (0.863–0.948)	0.946 (0.912–0.967)	0.966 (0.939–0.981)	0.886 (0.813–0.942)
75th	0.916 (0.833–0.947)	0.922 (0.878–0.941)	0.854 (0.767–0.905)	0.882 (0.814–0.921)
90th	0.926 (0.877–0.963)	0.871 (0.792–0.902)	0.856 (0.776–0.912)	0.926 (0.880–0.951)
Mean	0.935 (0.891–0.989)	0.927 (0.881–0.955)	0.826 (0.721–0.892)	0.915 (0.865–0.941)
Median	0.929 (0.857–0.967)	0.906 (0.847–0.941)	0.831 (0.762–0.921)	0.938 (0.898–0.962)
Kurtosis	0.919 (0.869–0.947)	0.930 (0.891–0.959)	0.862 (0.793–0.896)	0.925 (0.881–0.954)
Skewness	0.905 (0.848–0.942)	0.873 (0.801–0.918)	0.901 (0.846–0.936)	0.891 (0.831–0.926)

ADC apparent diffusion coefficient

expression in STS. Multifactorial analysis showed that necrosis over 50%, ADC$_{skewness}$, K^{trans}_{90th}, and FNCLCC grade III identified HIF-1alpha expression as the most promising predictors. In addition, HIF-1alpha expression above 75% may be associated with poorer OS and MFS.

Although various functional MRIs have been developed for evaluating the histological expression of solid tumors, conventional MRI sequences are still critical for radiologists. Several studies have illustrated that morphologic MRI characteristics may help predict pathological outcomes of STS. Zhao et al reported that peritumoral enhancement was an independent predictor of high-grade STS [36]. Crombé et al pointed out that MRI features, including necrosis, heterogeneity, and peritumoral enhancement of soft-tissue sarcomas, were associated with grade III tumors, metastasis-free survival, and overall survival [37]. In this study, the univariate results showed that the higher T2WI tumor heterogeneity and necrosis over 50% had significantly higher HIF-1alpha expression. Multifactorial analysis revealed that necrosis over 50% was an independent predictor of HIF-1alpha expression among all conventional MRI features. This finding was

very similar to that of Crombe. Indeed, HIF-1alpha reflects the oxygenation level of the tissue. For highly malignant sarcomas, the faster the growth rate, the higher the oxygen needs. When tumor neovascularization cannot meet its demand, necrosis is bound to occur. And the more extensive the area of necrosis, the higher the tumor's oxygen deprivation level will be. This malignant cycle explains why extensive necrosis tends to occur in sarcomas with high HIF-1alpha expression.

DWI detects the Brownian motion of water molecules and provides quantitative ADC parameters describing the level of tumor cellularization [38]. ADC has been initially applied to identify soft tissue tumor histologic grading, Ki-67 expression, and benign-malignant discrimination [30, 31, 39]. A recent study showed that whole-tumor ADC histogram parameters are valuable for differentiating between high- and low-grade STS, where skewness is an independent predictor of high-grade STS [40]. Our study showed that ADC$_{10th}$, ADC$_{25th}$, ADC$_{mean}$, and ADC$_{median}$ significantly decreased with increasing HIF-1alpha expression, while ADC$_{skewness}$ showed the most significant positive correlation trend. Although the increased area of tumor necrosis under hypoxia

Table 3 Measurements of histogram metrics derived by ADC, K^{trans}, K_{ep}, and V_e

Histogram metrics	ADC	K^{trans}	K_{ep}	V_e
10th	1.156 ± 0.271	0.081 ± 0.047	0.218 ± 0.176	0.156 ± 0.062
25th	1.263 ± 0.385	0.142 ± 0.057	0.473 ± 0.252	0.284 ± 0.152
75th	1.642 ± 0.552	0.472 ± 0.096	0.788 ± 0.365	0.571 ± 0.265
90th	1.827 ± 0.607	0.611 ± 0.166	0.914 ± 0.405	0.713 ± 0.309
Mean	1.581 ± 0.513	0.352 ± 0.144	0.621 ± 0.325	0.447 ± 0.257
Median	1.435 ± 0.435	0.291 ± 0.126	0.602 ± 0.314	0.413 ± 0.244
Kurtosis	2.564 ± 2.216	3.316 ± 2.741	1.563 ± 2.876	2.148 ± 3.123
Skewness	1.313 ± 1.781	0.524 ± 1.821	0.382 ± 0.733	0.422 ± 0.842

ADC apparent diffusion coefficient

Table 4 Correlations between quantitative MR parameters (ADC, K^{trans}, K_{ep}, and V_e) histogram metrics with HIF-1alpha expression in STS

| Parameters		rho	p value
ADC	10th	− 0.414	0.002*
	25th	− 0.379	0.005*
	75th	− 0.203	0.061
	90th	− 0.178	0.126
	Mean	− 0.271	0.026*
	Median	− 0.302	0.013*
	Kurtosis	0.196	0.218
	Skewness	0.526	< 0.001*
K^{trans}	10th	0.133	0.119
	25th	0.178	0.083
	75th	0.377	0.009*
	90th	0.427	0.002*
	Mean	0.324	0.012*
	Median	0.303	0.020*
	Kurtosis	0.145	0.208
	Skewness	− 0.352	0.005*
K_{ep}	10th	0.106	0.229
	25th	0.122	0.203
	75th	0.265	0.103
	90th	0.331	0.026*
	Mean	0.213	0.126
	Median	0.186	0.187
	Kurtosis	0.026	0.521
	Skewness	0.033	0.489
V_e	10th	0.109	0.337
	25th	0.165	0.131
	75th	0.142	0.242
	90th	0.030	0.817
	Mean	0.035	0.674
	Median	0.129	0.269
	Kurtosis	− 0.036	0.648
	Skewness	− 0.173	0.158

ADC apparent diffusion coefficient

*The result is statistically significant

may lead to an increase in voxels with high ADC values, the level of tumor cellularization is the determining factor leading to the formation of a hypoxic environment. This is because the induction pathway of HIF-1alpha in STS is mainly non-oxygen-dependent instead of an oxygen-dependent pathway [41]. This implies that HIF-1alpha expression primarily results from inducing oncogenic signals within tumor cells [42]. Therefore, higher levels of tumor cellularization may lead to increased expression of HIF-1alpha. Higher HIF-1alpha expression may promote glucose uptake and metabolism and enhance the proliferation of sarcoma cells, leading to an increase in cell number and volume, which may limit the

diffusion of water molecules, reflected by significantly lower ADC values [31]. The skewness reflects the asymmetry of the distribution, and the results of ADC_skewness reveal that STS with increased HIF-1alpha expression contains more voxels with ADC values lower than the average ADC. The results of the multifactorial analysis also confirmed that ADC_skewness was significantly better than the necrotic area in predicting HIF-1alpha expression.

DCE-MRI quantitative analysis introduces a pharmacokinetic model to monitor the interpenetration process between the contrast agent in the intravascular and extracellular extravascular space (EES), which allows a more accurate and visual description of microcirculatory information such as tumor tissue perfusion and capillary permeability [30]. In our study, multiple high-end percentiles and skewness of K^{trans} values, as well as K_{ep90th}, were correlated with HIF-1alpha expression, which is consistent with the findings of Xie and Awasthi in gliomas [17, 25]. The multifactorial analysis demonstrated that K^{trans}_{90th} might become an independent factor in predicting HIF-1alpha expression. It is known that HIF-1alpha induces the expression of downstream vascular-related factors such as VGEF, which means that high expression of HIF-1alpha leads to more tumor neovascularization [43]. The walls of these neovascular vessels are often incomplete and highly permeable. Therefore, the overall microcirculation level in the tumor is elevated, and the exchange of contrast agents between the vascular lumen and the EES is faster and more frequent, which could explain why the increased expression of HIF-1alpha leads to higher K^{trans} values. In this study, V_e values were not significantly correlated with HIF-1alpha expression, which is inconsistent with previous studies [25]. The V_e value reflects the volume of extracellular extravascular space. The acquisition of V_e values depends on steady-state equilibrium and requires a longer imaging time to be reliably measured. Therefore, it is difficult to estimate that the EES in tissues that have not yet been perfused and have not experienced extravascular contrast leakage may have contributed to the instability of V_e values.

We also explored the ability of histological features to predict HIF-1alpha expression. Unfortunately, the histological type may not predict HIF-1alpha expression, whereas the results of FNCLCC grading are exciting. Our results suggest that HIF-1alpha expression may be higher in high-grade sarcomas. FNCLCC grade III may significantly predict high HIF-1alpha expression and is second only to ADC_skewness. Indeed, the high heterogeneity within high-grade sarcomas and the abundant tumor blood supply could explain this result. There may be a significant association between the hypoxic microenvironment, tumor differentiation, and mitotic number. In addition, our preliminary analysis of the ability of HIF-1alpha expression to predict patient prognosis showed that patients had significantly
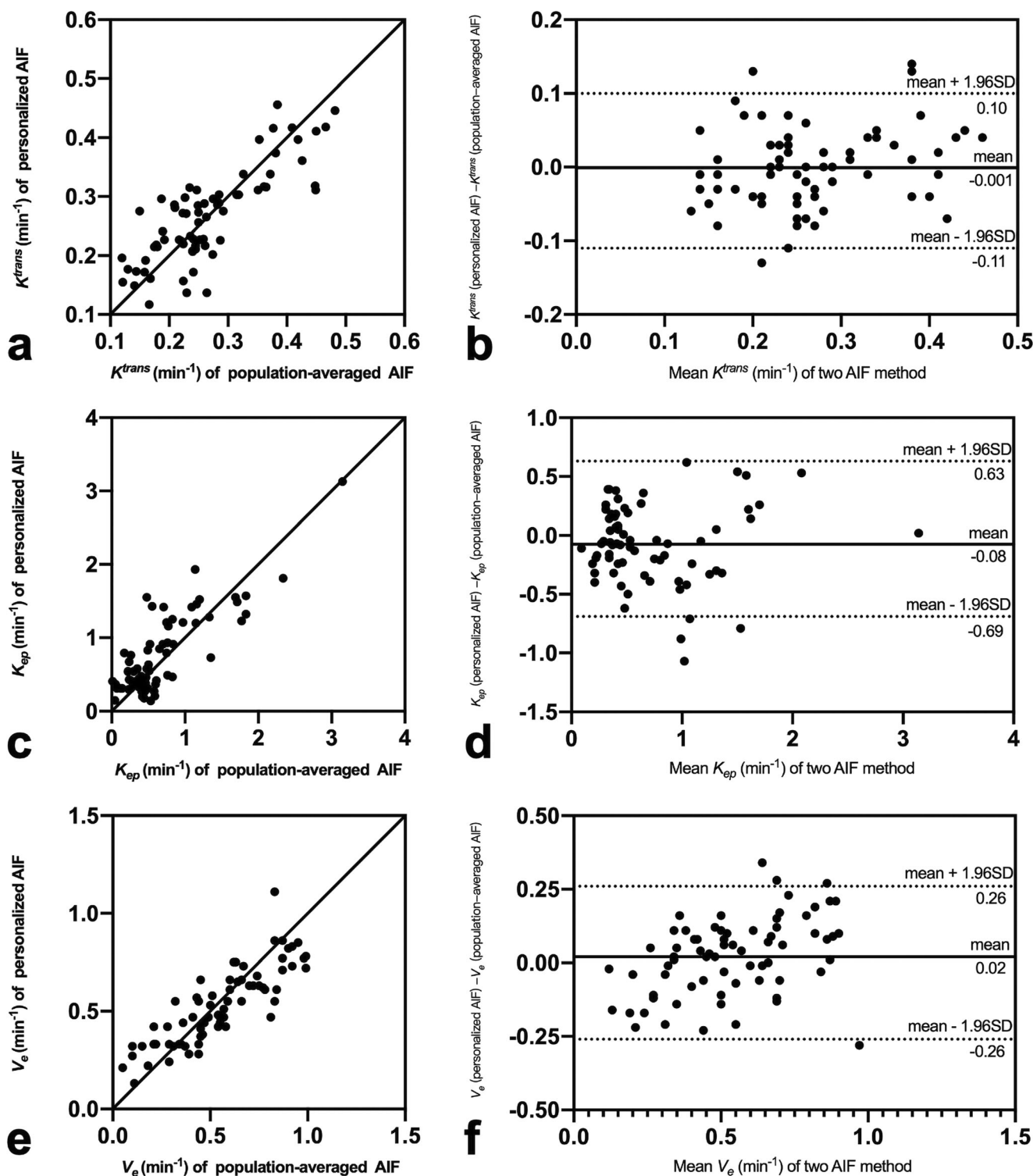
Fig. 2 Scatterplots and Bland-Altman plots of the personalized AIF method versus the population-averaged AIF method calculated for the DCE-MRI parameters. The scatterplots of K^{trans} (**a**), K_{ep} (**c**), and V_e (**e**) showed positive correlations ($r = 0.773$, $p < 0.001$; $r = 0.677$, $p < 0.001$; $r = 0.875$, $p < 0.001$). The mean measurement bias was -0.001 min^{-1} (95% consistency limit, -0.11 to 0.10 min^{-1}) for the K^{trans} value (**b**), -0.075 min^{-1} (95% consistency limit, -0.69 to 0.63 min^{-1}) for the K_{ep} value (**d**), and 0.20 min^{-1} (95% consistency limit, -0.26 to 0.26 min^{-1}) for the V_e value (**f**). The ICC values were 0.808 (95% confidence interval [CI] $0.709–0.876$) for the K^{trans} value, 0.820 (95% CI $0.726–0.884$) for the K_{ep} value, and 0.825 (95% CI $0.734–0.887$) for the V_e value
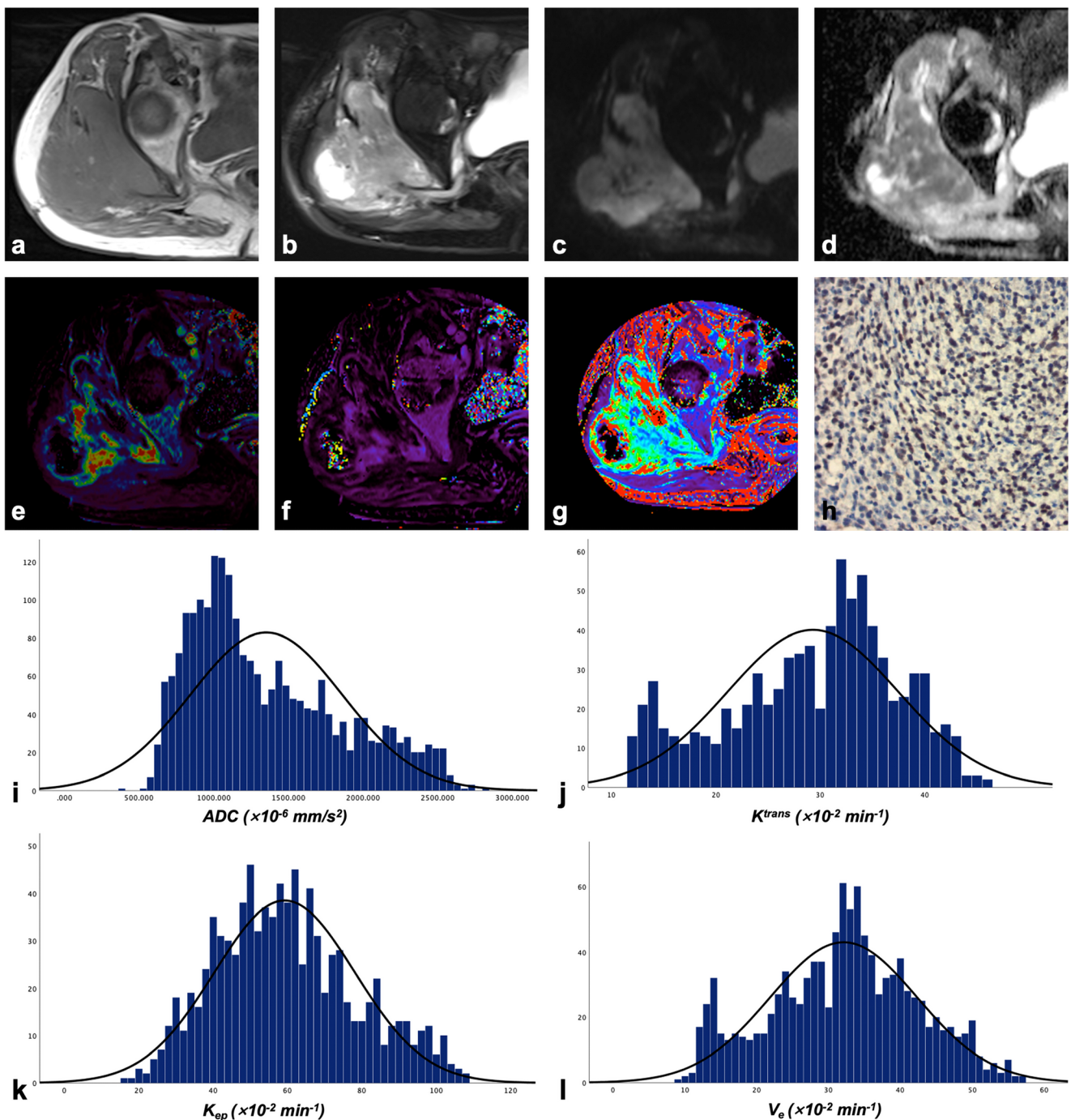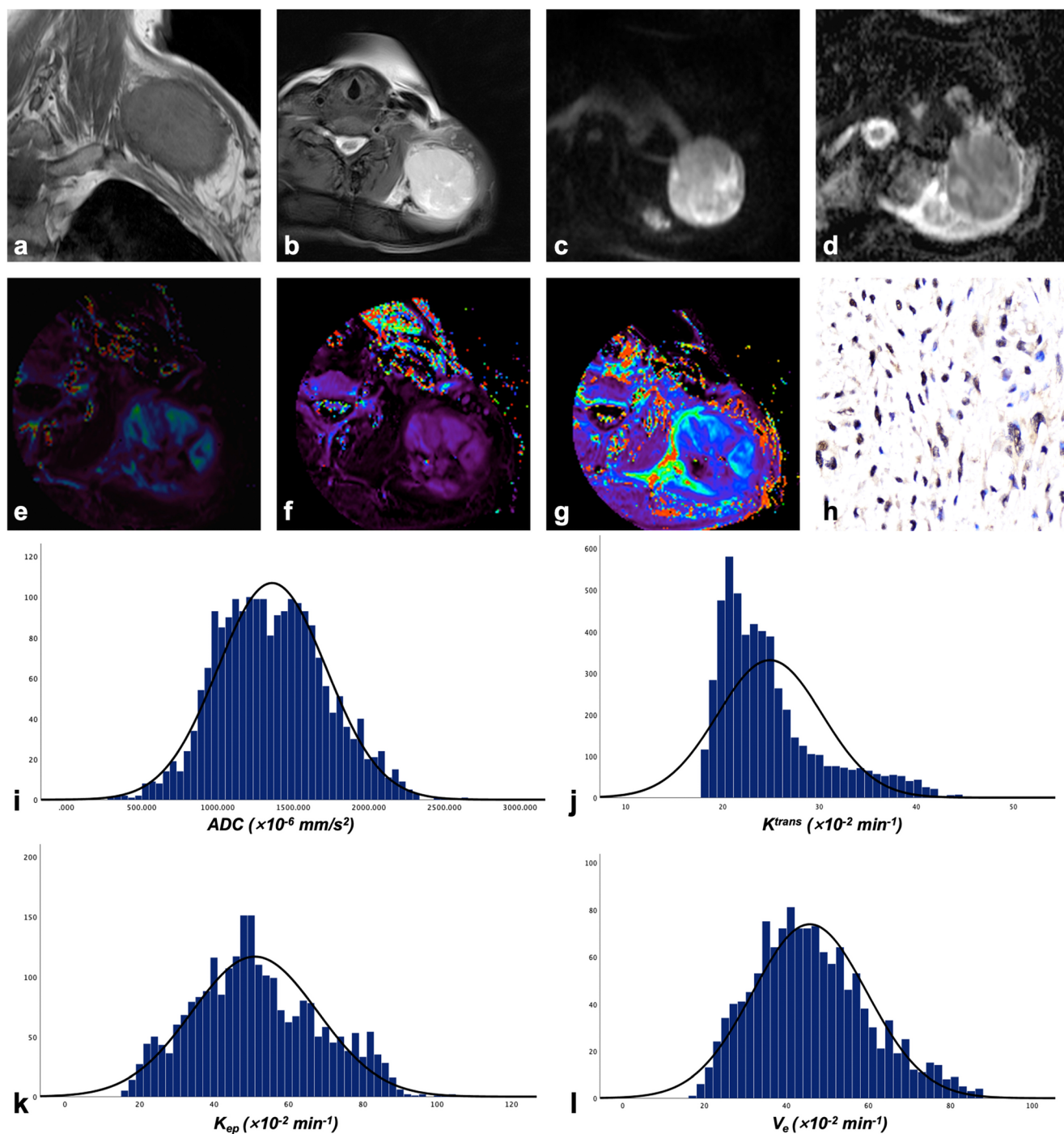
Fig. 3 MRI findings and histogram distributions of a 63-year-old male patient with extraskeletal osteosarcoma. The tumor shows equal muscle signal intensity on the T1-weighted image (**a**), high signal intensity on the T2-weighted image (**b**), and high signal intensity on the DWI ($b = 800$ s/mm^2) sequence (**c**). The ADC map demonstrated diffusion restriction (**d**). By DCE-MRI examination, the K^{trans} (**e**), K_{ep} (**f**), and V_e (**g**) maps were obtained. The ADC histogram (**i**) showed positive skewness, and the K^{trans} histogram (**j**) showed negative skewness. The K_{ep} (**k**) and V_e histograms (**l**) showed a normal distribution. Microscopic photographs at a magnification of 200 times showed that a large number of HIF-1α stained tumor cells were diffusely distributed. The final HIF-1alpha expression was determined to be 80% (**h**). The FNCLCC grade was grade III. Follow-up showed metastatic relapse 12 months after surgery, and the patient died of disease 4 months later

shorter OS and MFS when HIF-1alpha exceeded 75%. This indicates that HIF-1alpha can potentially be a biomarker of patient prognosis.

Several limitations should be considered when interpreting the results. First, this study has a small sample size and was conducted at a single institution. The differences in the

Fig. 4 MRI findings and histogram distributions of a 58-year-old female patient with myxoid liposarcoma. The tumor shows equal muscle signal intensity on the T1-weighted image (**a**), homogeneous high signal intensity on the T2-weighted image (**b**), and high signal intensity on the DWI ($b = 800$ s/mm^2) sequence (**c**). K^{trans} (**d**), K_{ep} (**e**), and V_e (**f**) maps were obtained from the DCE-MRI examination (**g**). The K^{trans} histogram (**j**) showed positive skewness. The ADC (**i**), K_{ep} (**k**), and V_e histograms (**l**) showed a normal distribution. Microscopic photographs at a magnification of 200 times showed that moderate amounts of HIF-1α stained tumor cells were diffusely distributed. The final HIF-1α expression was determined to be 30% (**h**). The FNCLCC grade was grade I

biological behavior of different histological types of STS may impact the final results. Second, the standardized image acquisition protocol in DCE-MRI imaging of STS remains uncertain. Further determination of the optimal DCE-MRI scanning protocol for STS is needed in the future. Third, the selection and processing of ROI in this study were singular. Texture analysis and deep learning may provide more in-depth information for image processing.

Table 5 Multiple linear regression analysis of MRI and histological features independently associated with HIF-1alpha expression in STS

MRI features	B coefficient	Standardized β coefficient	95% confidence interval	p value
Necrosis				
< 50% necrosis	0	–	–	
≥ 50% necrosis	1.352	0.074	0.715, 3.442	0.011*
$ADC_{Skewness}$	4.581	0.332	1.592, 7.413	0.003*
K^{trans}_{90th}	2.882	0.203	0.632, 5.783	0.027*
FNCLCC grade				
Grade I	0			
Grade II	2.131	0.093	0.437, 3.916	0.059
Grade III	4.473	0.314	1.417, 7.052	0.004*

ADC apparent diffusion coefficient

*The result is statistically significant

Fig. 5 Graphs show Kaplan-Meier survival curves for OS (**a**) and DFS (**b**) according to different HIF-1alpha groups categorized by quartiles and median
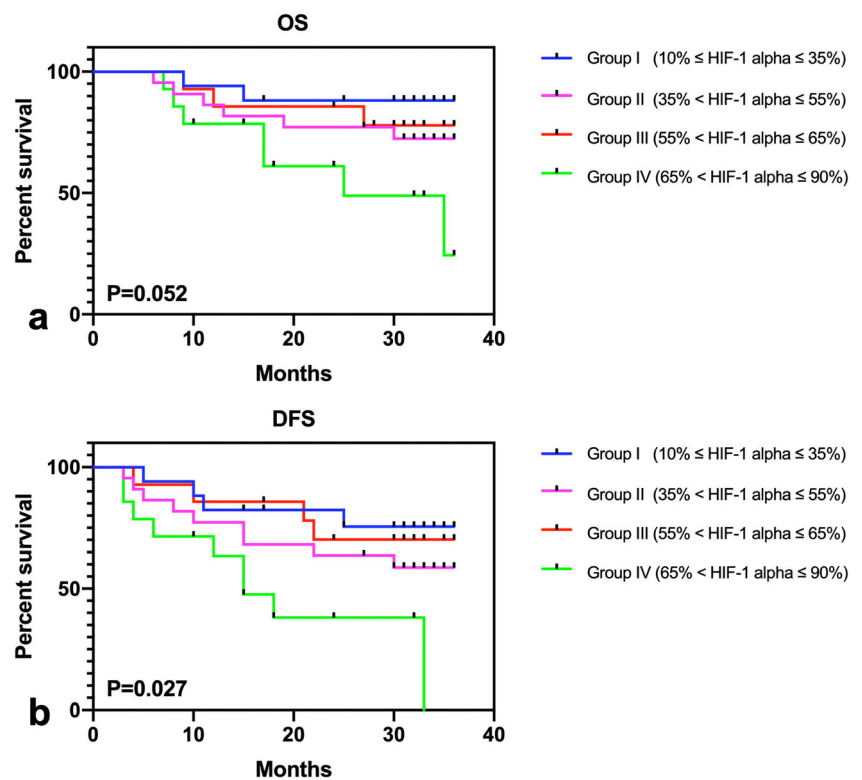
This study demonstrated a statistically significant correlation between DWI and DCE-MRI parameters histogram features and HIF-1alpha expression in STS. Morphological analysis of the lesions showed that more than 50% necrosis, $ADC_{skewness}$, K^{trans}_{90th}, and grade III were independently associated with HIF-1alpha expression. This result indicates the potential of conventional MRI combined with DWI and DCE-MRI analysis as imaging biomarkers for predicting the oxygenation level of STS. However, further extensive sample size studies are required to verify its true significance as an indirect prognostic predictor.

Declarations

Guarantor The scientific guarantor of this publication is Shuang Chen, PhD.

Conflict of interest One of the authors (Qing Li) is an employee of Siemens Healthcare. The remaining authors declare no relationships with any companies whose products or services may be related to the subject matter of the article.

Statistics and biometry No complex statistical methods were necessary for this paper.

Informed consent Written informed consent was obtained from all subjects in this study.

Ethical approval Institutional Review Board approval was obtained.

Methodology
• prospective
• case-control study/diagnostic study
• performed at one institution

References

1. Clark MA, Fisher C, Judson I, Thomas JM (2005) Soft-tissue sarcomas in adults. N Engl J Med 353:701–711
2. Merry E, Thway K, Jones RL, Huang PH (2021) Predictive and prognostic transcriptomic biomarkers in soft tissue sarcomas. NPJ Precis Oncol 5:17
3. Lugano R, Ramachandran M, Dimberg A (2020) Tumor angiogenesis: causes, consequences, challenges and opportunities. Cell Mol Life Sci 77:1745–1770
4. Hoos A, Stojadinovic A, Mastorides S et al (2001) High Ki-67 proliferative index predicts disease specific survival in patients with high-risk soft tissue sarcomas. Cancer 92:869–874
5. Seo HS, Lee H, Kim S et al (2021) Paravertebral muscles as indexes of sarcopenia and sarcopenic obesity: comparison with imaging and muscle function indexes and impact on cardiovascular and metabolic disorders. AJR Am J Roentgenol 216:1596–1606
6. Yang JP, Liao YD, Mai DM et al (2016) Tumor vasculogenic mimicry predicts poor prognosis in cancer patients: a meta-analysis. Angiogenesis 19:191–200
7. Semenza GL (2000) Hypoxia, clonal selection, and the role of HIF-1 in tumor progression. Crit Rev Biochem Mol Biol 35:71–103
8. Eubank TD, Roda JM, Liu H, O'Neil T, Marsh CB (2011) Opposing roles for HIF-1alpha and HIF-2alpha in the regulation of angiogenesis by mononuclear phagocytes. Blood 117:323–332
9. You L, Wu W, Wang X et al (2021) The role of hypoxia-inducible factor 1 in tumor immune evasion. Med Res Rev 41:1622–1643
10. Carmeliet P, Dor Y, Herbert JM et al (1998) Role of HIF-1alpha in hypoxia-mediated apoptosis, cell proliferation and tumour angiogenesis. Nature 394:485–490
11. Nystrom H, Jonsson M, Werner-Hartman L, Nilbert M, Carneiro A (2017) Hypoxia-inducible factor 1alpha predicts recurrence in high-grade soft tissue sarcoma of extremities and trunk wall. J Clin Pathol 70:879–885
12. Shintani K, Matsumine A, Kusuzaki K et al (2006) Expression of hypoxia-inducible factor (HIF)-1alpha as a biomarker of outcome in soft-tissue sarcomas. Virchows Arch 449:673–681
13. Eisinger-Mathason TS, Zhang M, Qiu Q et al (2013) Hypoxia-dependent modification of collagen networks promotes sarcoma metastasis. Cancer Discov 3:1190–1205
14. Masoud GN, Li W (2015) HIF-1alpha pathway: role, regulation and intervention for cancer therapy. Acta Pharm Sin B 5:378–389
15. Yoon C, Lee HJ, Park DJ et al (2015) Hypoxia-activated chemotherapeutic TH-302 enhances the effects of VEGF-A inhibition and radiation on sarcomas. Br J Cancer 113:46–56
16. Liang J, Cheng Q, Huang J et al (2019) Monitoring tumour microenvironment changes during anti-angiogenesis therapy using functional MRI. Angiogenesis 22:457–470
17. Awasthi R, Rathore RK, Soni P et al (2012) Discriminant analysis to classify glioma grading using dynamic contrast-enhanced MRI and immunohistochemical markers. Neuroradiology 54:205–213
18. Li X, Yang L, Wang Q, Tao J, Pan Z, Wang S (2021) Soft tissue sarcomas: IVIM and DKI correlate with the expression of HIF-1alpha on direct comparison of MRI and pathological slices. Eur Radiol 31:4669–4679
19. Liu M, Guo X, Wang S et al (2013) BOLD-MRI of breast invasive ductal carcinoma: correlation of R2* value and the expression of HIF-1alpha. Eur Radiol 23:3221–3227
20. Yin Z, Li X, Zhang Y et al (2022) Correlations between DWI, IVIM, and HIF-1alpha expression based on MRI and pathology in a murine model of rhabdomyosarcoma. Magn Reson Med 88:871–879
21. Jensen RL, Mumert ML, Gillespie DL, Kinney AY, Schabel MC, Salzman KL (2014) Preoperative dynamic contrast-enhanced MRI correlates with molecular markers of hypoxia and vascularity in specific areas of intratumoral microenvironment and is predictive of patient outcome. Neuro Oncol 16:280–291
22. Huang W, Zhang Q, Wu G et al (2021) DCE-MRI quantitative transport mapping for noninvasively detecting hypoxia inducible factor-1alpha, epidermal growth factor receptor overexpression, and Ki-67 in nasopharyngeal carcinoma patients. Radiother Oncol 164:146–154
23. Li X, Wu S, Li D et al (2019) Intravoxel incoherent motion combined with dynamic contrast-enhanced perfusion MRI of early cervical carcinoma: correlations between multimodal parameters and HIF-1alpha expression. J Magn Reson Imaging 50:918–929
24. Lindgren A, Anttila M, Rautiainen S et al (2019) Dynamic contrast-enhanced perfusion parameters in ovarian cancer: good accuracy in identifying high HIF-1alpha expression. PLoS One 14:e0221340
25. Xie Q, Wu J, Du Z et al (2019) DCE-MRI in human gliomas: a surrogate for assessment of invasive hypoxia marker HIF-1Alpha based on MRI-neuronavigation stereotactic biopsies. Acad Radiol 26:179–187
26. Borren A, Groenendaal G, van der Groep P et al (2013) Expression of hypoxia-inducible factor-1alpha and -2alpha in whole-mount prostate histology: relation with dynamic contrast-enhanced MRI and Gleason score. Oncol Rep 29:2249–2254
27. Huang Z, Xu X, Meng X et al (2015) Correlations between ADC values and molecular markers of Ki-67 and HIF-1alpha in hepatocellular carcinoma. Eur J Radiol 84:2464–2469
28. Swartz JE, Driessen JP, van Kempen PMW et al (2018) Influence of tumor and microenvironment characteristics on diffusion-weighted imaging in oropharyngeal carcinoma: a pilot study. Oral Oncol 77:9–15
29. Ma T, Yang S, Jing H et al (2018) Apparent diffusion coefficients in prostate cancer: correlation with molecular markers Ki-67, HIF-1alpha and VEGF. NMR Biomed 31
30. Choi YJ, Lee IS, Song YS, Kim JI, Choi KU, Song JW (2019) Diagnostic performance of diffusion-weighted (DWI) and dynamic contrast-enhanced (DCE) MRI for the differentiation of benign from malignant soft-tissue tumors. J Magn Reson Imaging 50:798–809
31. Lee JH, Yoon YC, Seo SW, Choi YL, Kim HS (2020) Soft tissue sarcoma: DWI and DCE-MRI parameters correlate with Ki-67 labeling index. Eur Radiol 30:914–924

32. Xiao Z, Tang Z, Zhang J et al (2020) Whole-tumor histogram analysis of monoexponential and advanced diffusion-weighted imaging for sinonasal malignant tumors: correlations with histopathologic features. J Magn Reson Imaging 51:273–285

33. Xie T, Zhao Q, Fu C et al (2019) Differentiation of triple-negative breast cancer from other subtypes through whole-tumor histogram analysis on multiparametric MR imaging. Eur Radiol 29:2535–2544

34. Khalifa F, Soliman A, El-Baz A et al (2014) Models and methods for analyzing DCE-MRI: a review. Med Phys 41:124301

35. Sourbron SP, Buckley DL (2013) Classic models for dynamic contrast-enhanced MRI. NMR Biomed 26:1004–1027

36. Zhao F, Ahlawat S, Farahani SJ et al (2014) Can MR imaging be used to predict tumor grade in soft-tissue sarcoma? Radiology 272:192–201

37. Crombe A, Marcellin PJ, Buy X et al (2019) Soft-tissue sarcomas: assessment of MRI features correlating with histologic grade and patient outcome. Radiology 291:710–721

38. Koh DM, Collins DJ (2007) Diffusion-weighted MRI in the body: applications and challenges in oncology. AJR Am J Roentgenol 188:1622–1635

39. Chhabra A, Ashikyan O, Slepicka C et al (2019) Conventional MR and diffusion-weighted imaging of musculoskeletal soft tissue malignancy: correlation with histologic grading. Eur Radiol 29:4485–4494

40. Kim BR, Kang Y, Lee J et al (2022) Tumor grading of soft tissue sarcomas: assessment with whole-tumor histogram analysis of apparent diffusion coefficient. Eur J Radiol 151:110319

41. Kim JI, Choi KU, Lee IS et al (2015) Expression of hypoxic markers and their prognostic significance in soft tissue sarcoma. Oncol Lett 9:1699–1706

42. Keith B, Johnson RS, Simon MC (2011) HIF1alpha and HIF2alpha: sibling rivalry in hypoxic tumour growth and progression. Nat Rev Cancer 12:9–22

43. Semenza GL (2002) HIF-1 and tumor progression: pathophysiology and therapeutics. Trends Mol Med 8:S62–S67

Publisher's note Springer Nature remains neutral with regard to jurisdictional claims in published maps and institutional affiliations.